

N-Type Doped Silicon Thin Film on a Porous Cu Current Collector as the Negative Electrode for Li-Ion Batteries

Aliya Mukanova,^[a] Arailym Nurpeissova,^[a] Sung-Soo Kim,^[b] Maksym Myronov,^[c] and Zhumabay Bakenov^{*[a]}

This work reports the preparation of a three-dimensional Si thin film negative electrode employing a porous Cu current collector. A previously reported copper etching procedure was modified to develop the porous structures inside a 9 μm thick copper foil. Magnetron sputtering was used for the deposition of an n-type doped 400 nm thick amorphous Si thin film. Electrochemical cycling of the prepared anode confirmed the ef-

fectiveness of utilizing the approach. The designed Si thin film electrode retained a capacity of around $67 \mu\text{Ah cm}^{-2}$ (1675 mAh g^{-1}) in 100th cycle. The improved electrochemical performance resulted in an enhancement of both areal capacity and capacity retention in contrast with flat and rough current collectors that were prepared for comparison.

1. Introduction

Over the last two decades, many studies have been devoted to the design of silicon-based negative electrodes for next-generation lithium-ion battery (LIB) technology. Researchers are motivated by a desire to move away from the traditional graphite anode with a specific capacity of 372 mAh g^{-1} to Si, owing to its high theoretical specific capacity of around 3579 mAh g^{-1} ,^[1] high volumetric capacity (2190 mAh cm^{-3}), low average delithiation potential (ca. 0.4 V vs. Li^+/Li), low potential hysteresis, and thus high energy efficiency.^[2,3] However, commercialization of this amazing material is delayed by an unsolved issue of its significant volume expansion (up to 280%) during the electrochemical reaction with lithium and the formation of lithiated $\text{Li}_{3.75}\text{Si}$ alloy. The mechanical stress occurring during alloying leads to degradation, cracking, and electrical contact loss in the electrode.^[4] Another resulting issue of Si expansion is the formation of a non-uniform thick solid electro-

lyte interphase (SEI), which obstructs the movement of Li^+ ions, leading to capacity fading.^[5] Various strategies have been employed to improve the electrochemical performance of Si. It has been observed that the decrease of Si particle size to the nanoscale prevents the cracking of particles.^[6] Amorphous phase Si (a-Si) has been found to be preferable over crystalline Si, because it experiences uniform expansion during the repetitive lithiation/delithiation reaction and mitigates the cracking of Si particles.^[4,7,8] Incorporation of dopants, especially n-type dopants, into Si materials leads to enhanced electron mobility.^[9,10] Among the investigated Si nanostructures (spheres, tubes, wires, etc.), Si thin films provide the ideal possibility to design high-capacity microscale LIBs.^[11–13] A 50 nm thick Si thin film electrode was reported to retain the highest stable specific capacity of 2000 mAh g^{-1} for 3000 cycles.^[10] However, to enhance the energy and power density in thin-film LIBs, the mass of active material should be increased. The issues of “thick” thin films (> 200 nm) are cracking (island formation^[14]) and delamination from the substrate, owing to the occurrence of strain–stress at the Si–substrate interface during lithiation. As previously reported, the soft and flexible substrates can be used to release emerging stress at the interface between the current collector and the thin films.^[15–18]


Three-dimensional (3D) structured Si thin film anodes are capable of accommodating the volume changes and releasing the tensile stress at the interface, thus reducing the delamination of the Si thin film.^[19] Moreover, this concept provides fast Li^+ diffusion, thereby remarkably increasing the volumetric capacity. Many attempts to optimize the shape of Si thin films (wires,^[20] ribbons,^[21] hills,^[22] patterns)^[23,24] and to modify the substrate surfaces^[25–27] have been performed and still continue, in order to improve the electrochemical battery performance and expand the battery cycle life.


Herein, we present a facile and cheap approach, employing a 3D porous Cu substrate, prepared by etching in ammonia so-

[a] A. Mukanova, Dr. A. Nurpeissova, Prof. Z. Bakenov
School of Engineering, National Laboratory Astana
Nazarbayev University
53 Kabanbay Batyr Ave., 010000, Astana (Kazakhstan)
E-mail: zbakenov@nu.edu.kz

[b] Prof. S.-S. Kim
Graduate School of Energy Science and Technology
Chungnam National University
99 Daehak ave., Yuseong-gu, Daejeon 34134 (South Korea)

[c] Prof. M. Myronov
Physics Department
University of Warwick
Coventry CV4 7AL (United Kingdom)

 The ORCID identification number(s) for the author(s) of this article can be found under <https://doi.org/10.1002/open.201700162>.

 © 2017 The Authors. Published by Wiley-VCH Verlag GmbH & Co. KGaA. This is an open access article under the terms of the Creative Commons Attribution-NonCommercial-NoDerivs License, which permits use and distribution in any medium, provided the original work is properly cited, the use is non-commercial and no modifications or adaptations are made.

lution, and magnetron sputtering (MS) for Si thin film deposition, which allowed us to obtain Si with an amorphous phase with n-type dopant impurities for enhancing electron conductivity. The porous substrate structure provided a high surface area and room for the volume expansion of Si. The substrate thickness was chosen to be as thin as possible (ca. 9 μm) in order to achieve a more flexible Si anode for the effective relaxation of emerging stress at the interface. The additional benefit is the lightweight and decreased thickness of the prepared anode, which is important for some applications, where the weight and dimensions of power source play an important role (i.e. medical implants, portable electronic devices, etc.). The electrochemical performance of the Si thin film anode on a 3D porous Cu substrate was compared with that of Si thin film anodes on flat and rough substrates to show the direct influence of the substrate surface conditions and the perspective of the applied concept.

2. Results and Discussion

The Raman spectrum of the obtained Si thin film is shown in Figure 1. The Raman spectrum exhibits the following peaks related to Si: the longitudinal optical mode of 310 cm^{-1} , the longitudinal acoustic mode of 400 cm^{-1} , the transverse optical mode at 480 cm^{-1} , and the overtone of the longitudinal and transverse phonons at around 650 cm^{-1} . The presence of these peaks allows us to conclude that the material sputtered on a Cu substrate is Si in an amorphous phase.^[28]

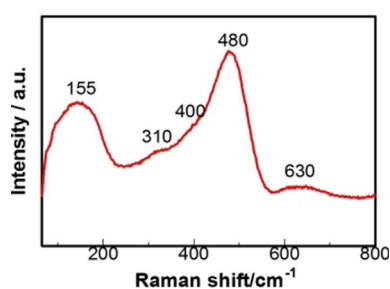


Figure 1. Raman spectrum of Si thin film.

Figure 2a shows the 3D AFM image of the edge of the Si thin film deposited on the polished glass (see the Experimental Section). The plot (Figure 2b) illustrates the thickness profile of

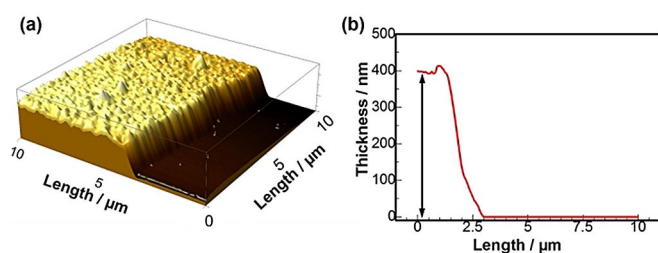


Figure 2. AFM mapping results. a) 3D image of thin film with edge illustration; b) the thickness profile of thin film.

the Si film to be around 400 nm, which was checked at several chosen points on the edge of the Si thin film. From the base of the AFM image, the average roughness of the Si thin film surface can be estimated to be within $\pm 25 \times 25\text{ nm}$ (width \times height).

SEM images are used to describe the morphology and structure of the Cu foils and Si thin film. Figure 3 illustrates the top-view images of Cu substrates with different surface conditions without (left column) and with a Si thin film (right column).

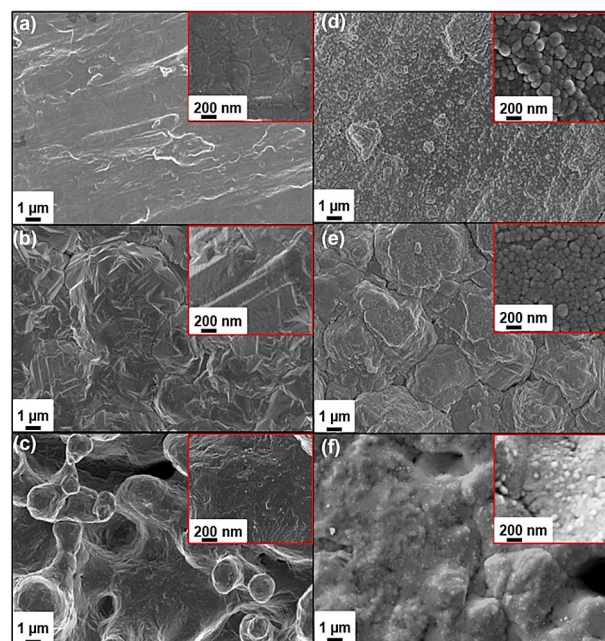


Figure 3. SEM images of substrates and Si on their surface: a) flat Cu; b) rough Cu; c) porous Cu; d) Si on flat Cu; e) Si on rough; f) Si on porous Cu.

The smooth surface for the flat Cu foil (Figure 3a) and hill-like formations on a surface of the rough foil (Figure 3b) can be observed. Figure 3c demonstrates the porous structure of the current collector. This resulting network with ledges and caves is a result of the reaction between copper and ammonia solution within the original solid structure; a slightly rough sample surface can be detected on the inserted image at higher magnification. Figure 3d–f illustrates the Si thin films deposited on the substrates. It can be seen that the thin film tends to repeat the substrate structure in the first (Figure 3d) and second case (Figure 3e), and almost completely fills the pores in the case of the porous current collector (Figure 3f). From the insets of the Si thin film images at higher magnification in Figure 3d–f, the spherical shape of the Si particles with a particle size up to 100 nm can be observed.

To evaluate the electrochemical performance of the Si thin film as an anode material, cycling voltammetry (CV) was used at a scan rate of 0.1 mVs^{-1} between 0 and 3 V. Three investigated Si thin film electrodes demonstrated similar patterns of Si lithiation/delithiation in the CV plot (Figure 4a). Considering the first cycle scans, it can be seen that the first electrochemical reaction occurred during discharging, and was detected at a

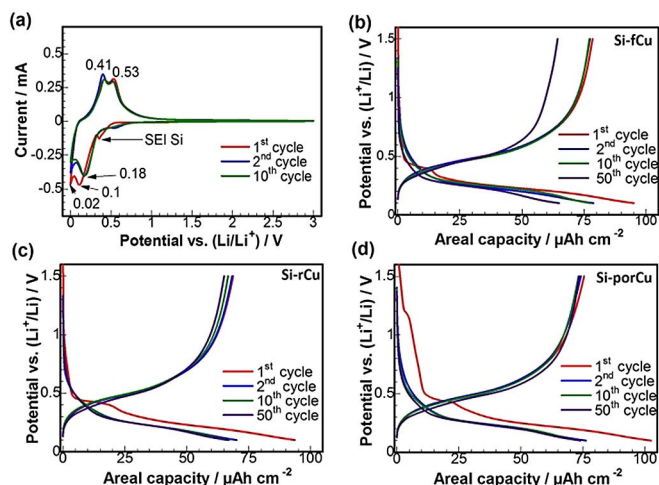


Figure 4. Electrochemical test results. a) CV for Si thin film at a scan rate of 0.1 mVs^{-1} between 0 and 3 V. Charge/discharge profile of Si thin film anode on b) flat, c) rough, and d) porous Cu foil. The current density was $30 \mu\text{Acm}^{-2}$ in the potential range of 0.1–1.5 V.

potential of 0.4 V. This is usually ascribed to the irreversible decomposition of electrolyte on the Si electrode surface, resulting in SEI layer formation.^[29] The cathodic peaks at 0.1 and 0.02 V indicate the first reversible lithiation reaction of Si and Li_xSi_y alloy formation. The corresponding delithiation reaction of Li_xSi_y back to Si is represented by the anodic peaks at 0.41 and 0.53 V.

The obtained peak positions are in a good agreement with the literature data for Si thin film anodes.^[30–32]

Figure 4b–d illustrates the potential profiles of the investigated anodes, recorded at a current density of $30 \mu\text{Acm}^{-2}$ in the potential range of 0.1–1.5 V. The first lithiation plateau occurred at a potential of around 0.4 V and was present for all samples. Observing the charge–discharge curves for flat (see Figure 4b) and rough (see Figure 4c) a-Si thin films, we can detect the initial discharge capacities around $95 \mu\text{Acm}^{-2}$ (2375 mAhg^{-1}) and $94 \mu\text{Acm}^{-2}$ (2350 mAhg^{-1}), respectively. In addition, the SEI formation process causes an irreversible capacity loss in the first cycle. Thus, the irreversible capacity loss constitutes 17 and $25 \mu\text{Acm}^{-2}$ for the flat and rough Si film anodes, respectively. By using a 3D porous substrate (Figure 4d) the performance of the a-Si thin film could be significantly enhanced. From Figure 4d, we can observe that the initial discharge capacity was increased to $102 \mu\text{Acm}^{-2}$ (2550 mAhg^{-1}). However, the irreversible capacity constituted approximately $27 \mu\text{Acm}^{-2}$ ($\text{ICE} = 75\%$), which is the highest among the three investigated anodes. The increased irreversible capacity loss in the 1st cycle in the case of both rough and porous substrates could be the result of increased surface area. The extended surface area possibly contains a higher amount of Cu oxide, which is involved in the process of SEI layer formation. This assumption can be confirmed by the noticeable plateau at 1.2 V (see Figure 4d), which corresponds to the reaction of Li ions with Cu oxide, the reduction of CuO to Cu, and the formation of Li_2O , all contributing to the SEI layer.^[33] From Figure 5, we can compare the capacity retentions

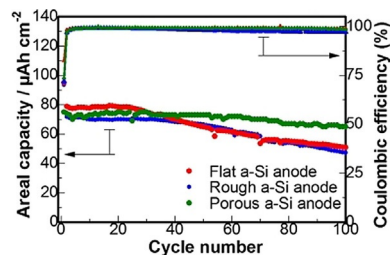


Figure 5. Cycling performance of the three a-Si thin film anodes. The current density was $30 \mu\text{Acm}^{-2}$ in the potential range of 0.1–1.5 V.

of the investigated samples. The flat anode retains the stable discharge capacity only until the 25th cycle, after which it rapidly decreases, achieving only $51 \mu\text{Acm}^{-2}$ (1250 mAhg^{-1}) in 100th cycle. The rough a-Si thin film exhibited a stable capacity of $70 \mu\text{Acm}^{-2}$ (1750 mAhg^{-1}) until the 40th cycle, followed by capacity fading to $47.4 \mu\text{Acm}^{-2}$ (1185 mAhg^{-1}) in the final cycle. It can be seen that the rough a-Si substrate shows better cycling stability upon cycling compared to the flat substrate; however, at the same time, both substrates showed a similar capacity value in the end. In contrast, a-Si on a porous substrate exhibits a significant improvement in stability throughout all cycles. The designed porous anode retained an areal charge capacity of $76.2 \mu\text{Acm}^{-2}$ (1905 mAhg^{-1}) until the 70th cycle, and then it slowly decreased to $67 \mu\text{Acm}^{-2}$ (1675 mAhg^{-1}) in the final cycle, losing 15% of the initial charge. For all investigated a-Si thin film anodes, the coulombic efficiency was within 97–99% in 100th cycle.

Figure 6 illustrates post-cycling SEM images of the samples. The post-cycling investigations of the flat Si anode (Figure 6a) revealed the extensive delamination of the Si thin film from the flat substrate with the remaining Si islands being around $15 \mu\text{m}$ in length. One can see that the islands' edges do not touch the substrate, indicating electrical contact loss. From the SEM images of the second anode (Figure 6b), we detected that the sputtered Si thin film experiences cracking, forming islands with approximately the same dimensions as those for Si on the flat substrate. However, the distances between islands are around few micrometers and the edges of the islands were

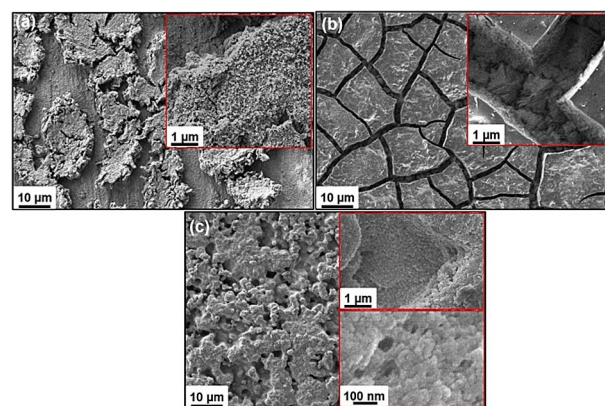


Figure 6. SEM images of samples after 100 cycles: a) a-Si on f-Cu; b) a-Si on r-Cu; c) a-Si on p-Cu.

not spoiled, which is in contrast with first anode. The Si sputtered on the porous substrate, shown in Figure 6c, did not exhibit significant mechanical failure of the thin film. No obvious cracks or open metallic regions with a bare surface were observed for this anode, which is in contrast with the other two examined samples. This could explain the improved capacity retention of a-Si on a porous substrate.

The comparison of the obtained results with published data, where similar concepts were employed (Si thin film anodes on metallic foams,^[34,35] Cu nanowires,^[36,37] cobalt nanosheet arrays,^[38] tobacco mosaic virus),^[39] is hampered by the difference in the thickness of the films, test conditions, number of cycles, and so on. Moreover, the deposition technique, preparation conditions, and electrolyte type can also significantly affect the electrochemical performance. The data summarized in existing reviews on Si-based anodes^[11,13,40] allowed us to conclude that our concept is more than compatible for further development, owing to a stable electrochemical performance of the material, even with increased thickness (and mass) of the Si thin film, and the low-cost preparation procedure.

3. Conclusions

In this study, we prepared a 3D porous Cu substrate from commercial Cu foil by etching in ammonia solution and it was used as a current collector for an a-Si thin film. The utilized strategy for improved anode performance included a 3D porous structure with increased surface area, the preparation of an n-type doped Si thin film in the amorphous phase, as well as annealing to enhance adhesion at the Si–Cu interface. Consequently, the designed electrode exhibited a remarkably improved electrochemical performance in contrast with flat and rough Si thin film anodes; the charge capacity was around $67 \mu\text{Ah cm}^{-2}$ (1675 mAh g^{-1}) over 100 cycles with 98.4% coulombic efficiency. We believe that the prepared porous thin Cu foil helped to successfully release the emerging stress and prevented the delamination of the Si thin film from the substrate; whereas, the porous structure was able to accommodate Si volume changes and provided a fast pathway for Li-ion diffusion. Thus, the concept employed in this work represents a step towards the design of lightweight Si thin film anodes with stable capacity retention.

Experimental Section

Anode Preparation

A porous substrate was prepared from commercially available Cu foil (9 μm , 99.9%, MTI) by using a procedure based on etching with ammonia solution. This method was utilized for the growth of Cu nanowires on a 25 μm thick Cu surface.^[41] To obtain the desirable porous structure, a series of modifications were made to the procedure. Firstly, the time of etching was decreased to 18 h, as the Cu foil used in our work was thinner and tended to be destroyed at the longer etching times. Secondly, the annealing temperature was lowered to 300 °C with prolongation of the Cu(OH)₂ reduction step to 14 h, owing to the same reasons as for etching. Finally, reduced Cu nanowires were easily removed from the sur-

face and pores after ultrasonication for 10 s followed by washing in deionized water and drying. The mass of the etched Cu foil constituted 5.7 mg cm^{-2} with a loss of one third of its initial mass. The 9 μm current collector is thinnest one of all the substrates reported for Si thin films. The conditions presented above for Cu foil etching resulted from the optimization and allowed us to prepare a thin porous Cu substrate, which is mechanically stable during handling.

The N-type doped 400 nm a-Si film was deposited on a Cu substrate (9 μm , MTI) with different surface conditions by using a radio frequency magnetron sputtering system (Kurt J. Lesker Company) and a 0.5 cm thick n-doped Si target (Kurt J. Lesker Company) that measured 5 cm in diameter. The magnetron sputtering was performed in a vacuum chamber under a pressure of 0.67 Pa in an inert atmosphere of Ar for 1 h at a power of 80 W. The substrate was rotated at 5 min^{-1} to evenly distribute the Si deposition, the tilt angle was around 30°. The mass of sputtered Si was determined by using a microbalance MSE2.7S-000-DM (Sartorius) before and after sputtering, and was measured to be around $0.04 \pm 0.002 \text{ mg cm}^{-2}$, being equal for all three sample types.

Before battery assembly, the anodes went through an annealing process inside the high-temperature tube furnace STF 1200 (Across International) at 150 °C for 60 min to remove condensed water particles from the surface of the anode. The temperature of annealing was further increased to 300 °C to remove oxides, which have adverse effect on the performance of batteries. The annealing step at 300 °C lasted for another 60 min. The annealing in both cases was performed under the constant flow of $150 \text{ cm}^3 \text{ min}^{-1}$ Ar + (5%) H₂. Owing to the inter-diffusion of Si and Cu at the interface between the two layers, annealing strengthens the adhesion between the Si film and the substrate. This is known to positively affect the performance of batteries.^[42]

Characterization

The obtained thin films were characterized on a LabRAM HR Evolution Raman spectroscope (HORIBA) at a laser wavelength of 532 nm. Scanning electron microscopy (SEM) images were taken by using a Crossbeam 540 (ZEISS). The thin film thickness measurement was performed by using atomic force microscopy (AFM) on a C3M SmartSPM™-1000 (AIST-HT) in tapping mode with an Al reflective side cantilever (NSG30 SS by TipsNano) measuring 125 μm in length and with a resonant frequency of 200–440 kHz. The samples for AFM were prepared on polished glass with the marker line drawn on its surface prior to sputtering, which was then easily removed with ethanol.

Electrochemical Testing

Electrochemical experiments were performed by using CR2032 coin cells (MTI corp.) assembled in an Ar-filled glovebox LABmaster Pro (MBRAUN, Glovebox, < 0.1 ppm H₂O and O₂). A lithium metal chip (99.9%, MTI corp.) served as the counter and reference electrode. 1 M LiPF₆ in a mixture of ethylene carbonate, diethyl carbonate, and ethyl methyl carbonate (1:1:1 v/v) was used as the electrolyte (5 drops), and porous polypropylene (Celgard® 2400) was employed as a separator. Galvanostatic charge/discharge tests were carried out on an Arbin BT-2000 battery tester between 1.5 and 0.1 V at approximately $30 \mu\text{A cm}^{-2}$ at ambient temperature. All potentials given in the paper are referenced to Li⁺/Li. The capacity is presented in $\mu\text{Ah cm}^{-2}$, using an electrode with a surface of 15.5 mm in diameter; the specific capacity is provided in brackets.

Acknowledgements

The authors acknowledge financial support from the Ministry of Education and Science of the Republic of Kazakhstan (Targeted program No. 0115PK03029 "NU-Berkeley strategic initiative in warm-dense matter, advanced materials and energy sources for 2014–2018"). A.M. thanks the PhD Program Grant from the Ministry of Education and Science of the Republic of Kazakhstan. The publication cost of this paper was supported by the National Laboratory Astana, Nazarbayev University.

Conflict of Interest

The authors declare no conflict of interest.

Keywords: lithium-ion batteries · magnetron sputtering · n-type doped silicon · porous current collector · thin films

- [1] A. Reyes Jiménez, R. Klöpsch, R. Wagner, U. C. Rodehorst, M. Kolek, R. Nölle, M. Winter, T. Placke, *ACS Nano* **2017**, *11*, 4731–4744.
- [2] P. Meister, H. Jia, J. Li, R. Kloepsch, M. Winter, T. Placke, *Chem. Mater.* **2016**, *28*, 7203–7217.
- [3] M. N. Obrovac, L. J. Krause, *J. Electrochem. Soc.* **2007**, *154*, A103–A108.
- [4] B. Gattu, R. Epur, P. M. Shanti, P. H. Jampani, *Inorg. Art.* **2017**, *5*, 1–14.
- [5] F. Holtstiege, A. Wilken, M. Winter, T. Placke, *Phys. Chem. Chem. Phys.* **2017**, *19*, 25905–25918.
- [6] X. H. Liu, L. Zhong, S. Huang, S. X. Mao, T. Zhu, J. Y. Huang, *ACS Nano* **2012**, *6*, 1522–1531.
- [7] S. Bourderau, T. Brousse, D. Schleich, *J. Power Sources* **1999**, *81*–82, 233–236.
- [8] A. Casimir, H. Zhang, O. Ogoko, J. C. Amine, J. Lu, G. Wu, *Nano Energy* **2016**, *27*, 359–376.
- [9] J. O. Song, H. T. Shim, D. J. Byun, J. K. Lee, *Adv. Nanomater. Process.* **2007**, *124–126*, 1063–1066.
- [10] T. Takamura, S. Ohara, M. Uehara, J. Suzuki, K. Sekine, *J. Power Sources* **2004**, *129*, 96–100.
- [11] U. Kasavajjula, C. Wang, *J. Power Sources* **2007**, *163*, 1003–1039.
- [12] M. N. Obrovac, V. L. Chevrier, *Chem. Rev.* **2014**, *114*, 11444–11502.
- [13] X. Zuo, J. Zhu, P. Müller-Buschbaum, Y.-J. Cheng, *Nano Energy* **2017**, *31*, 113–143.
- [14] J. P. Maranchi, A. F. Hepp, P. N. Kumta, *Electrochem. Solid-State Lett.* **2003**, *6*, A198.
- [15] S. H. Patel, Numerical Modeling of the Failure Mechanisms in Si Thin Film Anode for Li-Ion Batteries, Michigan Technological University, **2011**.
- [16] J. Shaffer, P. Peralta, Finite Element Analysis of Silicon Thin Films on Soft Substrates as Anodes for Lithium Ion Batteries, Arizona State University, **2011**.
- [17] J. Li, A. K. Dozier, Y. Li, F. Yang, Y.-T. Cheng, *J. Electrochem. Soc.* **2011**, *158*, A689.
- [18] H. B. Chew, B. Hou, X. Wang, S. Xia, *Int. J. Solids Struct.* **2014**, *51*, 4176–4187.
- [19] J. F. M. Oudenhoven, L. Baggetto, P. H. L. Notten, *Adv. Energy Mater.* **2011**, *1*, 10–33.
- [20] C. K. Chan, R. Ruffo, S. S. Hong, Y. Cui, *J. Power Sources* **2009**, *189*, 1132–1140.
- [21] C. Yu, X. Li, T. Ma, J. Rong, R. Zhang, J. Shaffer, Y. An, Q. Liu, B. Wei, H. Jiang, *Adv. Energy Mater.* **2012**, *2*, 68–73.
- [22] T. Zhang, H. P. Zhang, L. C. Yang, B. Wang, Y. P. Wu, T. Takamura, *Electrochim. Acta* **2008**, *53*, 5660–5664.
- [23] G. Cho, J. Noh, H. Sung, S. Lee, Y. Im, H. Ahn, K. Kim, *Nanoscale Res. Lett.* **2012**, *7*, 20.
- [24] G.-B. Cho, J.-K. Kim, S.-H. Lee, G.-T. Kim, J.-P. Noh, K.-K. Cho, K.-W. Kim, T.-H. Nam, H.-J. Ahn, *Electrochim. Acta* **2017**, *224*, 649–659 <https://doi.org/10.1016/j.electacta.2016.12.067>.
- [25] S. K. J. H. X. Deng, C. Y. Chung, M. Park, C. H. Park, *ECS Trans.* **2007**, *2*, 105–112.
- [26] J. B. Kim, B. S. Jun, S. M. Lee, *Electrochim. Acta* **2005**, *50*, 3390–3394.
- [27] G. B. Cho, J. K. Kim, S. H. Lee, G. Kim, J. Noh, K. Cho, K. Kim, T. Nam, H. Ahn, *Electrochim. Acta* **2016**, *224*, 649–659.
- [28] V. Baranchugov, E. Markevich, E. Pollak, G. Salitra, D. Aurbach, *Electrochem. commun.* **2007**, *9*, 796–800.
- [29] C. Li, C. Liu, W. Wang, Z. Mutlu, J. Bell, K. Ahmed, R. Ye, M. Ozkan, C. S. Ozkan, *Sci. Rep.* **2017**, *7*, 917.
- [30] T. D. Hatchard, J. R. Dahn, *J. Electrochem. Soc.* **2004**, *151*, A838–A842.
- [31] D. Ma, Z. Cao, A. Hu, *Nano-Micro Lett.* **2014**, *6*, 347–358.
- [32] P. Limthongkul, Y. Il Jang, N. J. Dudney, Y. M. Chiang, *J. Power Sources* **2003**, *119–121*, 604–609.
- [33] J. Tarascon, P. Poizot, S. Laruelle, S. Grugeon, L. Dupont, *Nature* **2000**, *407*, 496–499.
- [34] M. Haro, V. Singh, S. Steinhauer, E. Toulkeridou, *Adv. Sci.* **2017**, *4*, 1700180.
- [35] F. Dogan, L. D. Sanjeeva, S. J. Hwu, J. T. Vaughey, *Solid State Ionics* **2015**, *288*, 204–206.
- [36] R. Lin, S. Zhang, Z. Du, H. Fang, Y. Ren, X. Wu, *RSC Adv.* **2015**, *5*, 87090–87097.
- [37] K. Xu, Y. He, L. Ben, H. Li, X. Huang, *J. Power Sources* **2015**, *281*, 455–460.
- [38] X. H. Huang, J. B. Wu, Y. Q. Cao, P. Zhang, Y. Lin, R. Q. Guo, *Electrochim. Acta* **2016**, *203*, 213–220.
- [39] X. Chen, K. Gerasopoulos, J. Guo, A. Brown, C. Wang, R. Ghodssi, J. N. Culver, *Adv. Funct. Mater.* **2011**, *21*, 380–387.
- [40] J. R. Szczech, S. Jin, *Energy Environ. Sci.* **2011**, *4*, 56.
- [41] C. Yang, Y. Yin, S. Zhang, N. Li, Y. Guo, *Nat. Commun.* **2015**, *6*, 8058.
- [42] L. B. Chen, J. Y. Xie, H. C. Yu, T. H. Wang, *J. Appl. Electrochem.* **2009**, *39*, 1157–1162.

Received: October 14, 2017

Version of record online December 7, 2017